

# Highly Accelerated 3D Amide Proton Transfer (APT) Imaging of the Whole Brain at 3T Using a 32-Channel Phased-Array Coil

H. Zhu<sup>1,2</sup>, C. K. Jones<sup>1,2</sup>, J. Hua<sup>1,2</sup>, R. Ouwerkerk<sup>1</sup>, P. C. van Zijl<sup>1,2</sup>, P. Barker<sup>1,2</sup>, and J. Zhou<sup>1,2</sup>

<sup>1</sup>Department of Radiology, Johns Hopkins University, Baltimore, Maryland, United States, <sup>2</sup>F.M. Kirby Research Center for Functional Brain Imaging, Kennedy Krieger Institute, Baltimore, Maryland, United States

## Introduction

Recently, a new MRI contrast mechanism, called chemical exchange saturation transfer (CEST)<sup>1-3</sup>, has emerged in the field of molecular imaging. This contrast is generated by saturation labeling of exchangeable protons on the agent, followed by chemical exchange of this label to water protons. Amide proton transfer (APT) imaging is a specific type of CEST imaging that gives contrast due to endogenous cytosolic protein and peptide content<sup>4</sup>, as well as tissue pH<sup>5</sup>, *in vivo*. The clinical application of APT to neuroimaging is promising but to date remains limited to single-slice<sup>4</sup>. The underlying reasons for these limitations include the long scan time, potentially high power deposition, B<sub>0</sub> and B<sub>1</sub> field homogeneity, and interference of multiple saturation effects. To address these issues, we here present a 3D gradient and spin echo (GRASE) approach for whole-brain APT imaging, using SENSE accelerations in two directions enabled by a 32-channel phased-array head coil.

## Materials and Methods

Experiments were performed on a Philips Achieva 3T MRI scanner (R2.6.1) using a proto-type 32-channel phased-array coil for reception (Invivo, Inc., Florida). A rapid B<sub>0</sub>/B<sub>1</sub> mapping method was used to numerically optimize B<sub>0</sub> shimming parameters and B<sub>1</sub> scale. The GRASE 3D sequence (Fig. 1) consisted of three sections: RF saturation (840 ms), lipid suppression (20 ms) and GRASE 3D image acquisition (440 ms). The RF saturation section, configured to meet limitations of the RF amplifier, included four identical units, each consisting of a RF block pulse (200ms duration and 2μT amplitude) and a crusher gradient (10ms duration and 10mT/m strength). Lipid suppression was achieved with an asymmetric frequency modulated (FM) suppression pulse (102° flip and 17.6ms duration) and a crusher gradient. The sharper cutoff edge of the FM suppression pulse, when compared to a symmetric Gaussian pulse, enabled the suppression band to cover a wider range of *in vivo* lipid spectrum without affecting water signal. The GRASE 3D image acquisition was configured with a TSE factor of 22 in RL and an EPI factor of 7 in FH. FOV = 212mm(AP)×186mm(RL) with 2.2mm×2.2mm resolutions. 30 slices of 4.4 mm thickness covered 132 mm in the FH direction. With SENSE acceleration factors of 2×2 in RL and FH, the actual imaging matrix was 96(AP)×44(RL)×28(FH). Profile ordering in RL was set to low-high. Each 3D volume was acquired by 8 acquisitions (2 in RL and 4 in FH). The imaging time for one whole volume at each frequency offset was 2.5s×8 = 20s that resulted in a total scan time of 8:40 for a typical 30-slice, 26-offset z-spectrum protocol. SAR was 1.2w/kg, well within FDA guidelines.

## Results

Fig. 2 shows images without (M<sub>0</sub>) and with (±3.5ppm) RF saturation, and APT images (calculated using the magnetization transfer ratio-asymmetry at ±3.5ppm:  $MTR_{asym}(3.5ppm) = 100\% \times [M_{sat}(-3.5ppm) - M_{sat}(3.5ppm)] / M_0$ ) for three typical slices, acquired without lipid suppression. The saturated images at the offset of 3.5ppm had a high signal-to-noise ratio of 45 to 50. The artifacts on the APT images are clearly visual, including those caused by B<sub>0</sub> field inhomogeneity (slice a, black arrow) in regions near air-tissue interfaces (sinus, ear), and those caused by lipid (slice c, white arrow) on the top of the brain. When acquiring the APT reference image at -3.5ppm (1.2ppm in the proton spectrum), the lipid signal is suppressed. However, there is no lipid suppression when saturating the amide protons at +3.5ppm, so the asymmetry analysis leads to a fat artifact. Fig. 3 shows the whole-brain APT images for a healthy subject, acquired with FM lipid suppression and corrected for B<sub>0</sub> field inhomogeneity. There were several ways to correct for the B<sub>0</sub> inhomogeneity-related artifacts. Here, we acquired the full z-spectrum (-6 to 6ppm, interval 0.5ppm), and the artifacts were corrected through the fitting of the z-spectrum and re-assignment of the water center frequency<sup>4</sup>. Because the lipid resonance was suppressed equally at both offsets ±3.5ppm, appropriate APT images were obtained, except 2-3 top slices, where the lipid signal dominated and some residual lipid artifacts were still visual.

## Discussion

The 3D GRASE readout offers important advantages for whole-brain APT applications. First, the APT contrast for the entire imaging volume was recorded by one 90° excitation pulse shortly after RF saturation. Each line of k-space data acquired after the excitation contributes to all reconstructed images uniformly. Multi-slice acquisition, on the other hand, would suffer from decaying APT contrasts from slice to slice caused by time-dependent saturation loss. Secondly, a 3D acquisition allows SENSE accelerations in two directions that are enabled by modern high density phased-array coils. Together with the EPI factor, TSE factor, and SENSE factor, this allows the whole brain to be imaged with a highly efficient data acquisition scheme.

In conclusion, our *in vivo* results have demonstrated the feasibility of a time-efficient, whole-brain APT imaging technique at 3T for clinical applications. This technique combines an efficient 3D GRASE readout with 2D SENSE accelerations. The 3D GRASE approach can be applied to other types of CEST imaging applications.

**References:** (1) Ward et al. JMR 2000;143:79. (2) Zhang et al. JACS 2001;123:1517. (3) Aime et al. MRM 2002;47:639. (4) Zhou et al. MRM 2008;60:842. (5) Sun et al. JCBFM 2007;27:1129.

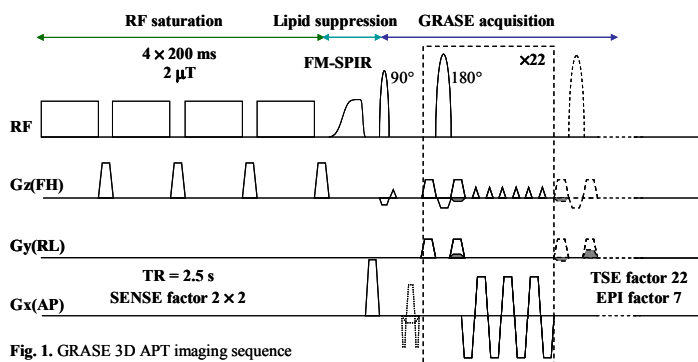


Fig. 1. GRASE 3D APT imaging sequence

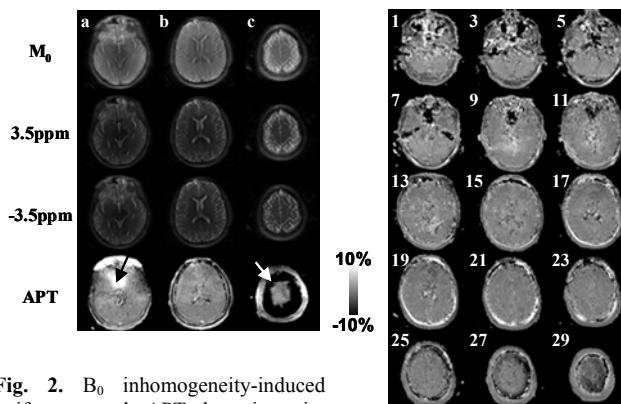


Fig. 2. B<sub>0</sub> inhomogeneity-induced artifact caused APT hyperintensity (black arrow in slice a). Lipid artifacts caused ring-like APT hypointensity (white arrow in slice c).

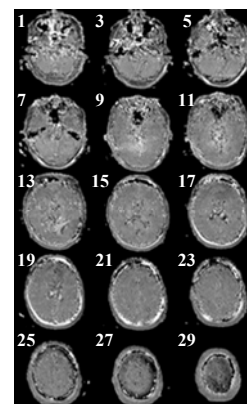


Fig. 3. With lipid suppression and B<sub>0</sub> correction, all APT images of the whole brain (odd slices shown only) were reasonably homogeneous.